5.4 The Effect of Post-Weld Mechanical Dressing

5.4.1 Ground specimens

A total of six specimens, in which the continuous welds had been burr-ground, were supplied for testing. Three of the test specimens were fabricated from BS 4360 grade 55E, and three from the higher strength ROQ-tuf AD 690. It had been proposed by the fan manufacturers that a weld fabricated using a 309 L austenitic stainless steel electrode would help eliminate any potential hydrogen pick-up by the carbon manganese base material (109). Accordingly, two of the ground specimens (one 55E and one AD 690) were made using the 309 L electrode, such that the fatigue strength of this detail could be evaluated.

The results of the fatigue tests performed on the six ground welds are summarised in Table 5.6, and it is clear that there is a significant improvement in fatigue strength, compared to the as-welded specimens (Table 5.3). It is also evident that the 309 L welds do not have a great effect on the fatigue strength of this detail, although it can be seen that specimen T27 recorded the lowest crack initiation stress range of 150 MPa. However, as will be detailed in the following Chapter, examination of the fracture surface indicated that the initiation had occurred from a small surface defect near the weld toe, whereas in the other five ground specimens the initiation site was removed from the weld toe to the weld root. This is considered a crucial point: if the weld dressing is not adequately performed, the fatigue strength of the detail may not be increased at all. However, an endurance limit of 160 MPa can be obtained if the welds are properly ground. The anomalously high result obtained for specimen T15 is due to the fact that this test was started at a stress range of 60 MPa, and the actual endurance limit of the detail was enhanced by coaxing. (Subsequent tests on the dressed specimens were started at an initial stress range of 160 MPa).

5.4.2 Peened specimens

A total of nine continuously welded specimens were supplied for testing; the weld toes of these welds had been peened using three passes with a single point (10 mm diameter) pneumatic hammer. Five of these specimens were fabricated using the E7018 electrode (three from 55E and two from AD 690), and four using the 309 L electrode (two 55E and two AD 690). The results are summarised in Table 5.7, and it is clear from this Table that the cold-working of the weld toe has a very significant effect on the fatigue strength of this detail. It is also evident that the peening operation must be carried out with some considerable care; if the tool is not directed accurately onto the weld toe, initiation can still occur from weld toe defects, as was the case in specimens T23 and T29. It is also evident that at these high stress ranges, crack initiation can occur remote from the weld (as in the case of specimens T22 and T24), where crack initiation occurred from the flame cut edge of the load bearing plate. It has in fact been shown (95) that micro cracks can originate at plate edges from even high quality gas-cutting.

However, the fatigue strength of the peened detail was shown to be in excess of 200 MPa, provided the weld toe is sufficiently cold worked, and that there were no other preferential crack initiation sites in the vicinity of the weld. The anomolously high values recorded for specimens T19 and T20 are again due to a relatively low starting stress range; thus the endurance limit recorded for these specimnens was enhanced by coaxing. The results obtained in the peened specimens also indicate that the 309 L stainless steel weld does not affect the fatigue strength of this detail to any great extent.

5.5 Summary

This test programme has shown how the fatigue strength of non-load carrying fillet welds can be improved significantly by cost-effective procedures such as grinding and hammer peening. The results obtained in the test programme are summarised in Figure 5.9, where it can be seen that the endurance limit of the stitch and continuously welded specimens is 50 MPa. In the case of the continuous welds, which were thought to represent an improvement over the stitch welded detail, small undercut defects at the weld toes led to fatigue crack initiation at relatively low stress ranges. If these welds are poorly fabricated, i.e. using high welding currents and welding without a pre-heat, a hard near-heat affected zone acts synergistically with the undercut defects to lower the endurance limit (as defined in Section 5.2) to 40 MPa.

The results of the tests carried out at high mean stress levels indicated that while the reduction of residual stresses by heat treatment can be an effective method of increasing the tolerance of a welded structure to brittle fracture, it may well be relatively ineffective in increasing the fatigue life of that structure.

Effective removal of the preferential crack initiation sites at the weld toes by grinding increases the endurance limit of this detail to 160 MPa. If the weld toe is effectively cold worked by peening, such that the preferential crack initiation sites are removed and a residual surface compressive stress is generated, the endurance limit is increased to more than 200 MPa. At these high stress ranges, however, cracking can initiate from flame cut edges remote from the weld, thus illustrating the effectiveness of these mechanical dressing techniques in improving the fatigue strength of the weld.

Both mechanical dressing techniques should be implemented with care, however. In the limited number of specimens tested in this work, two peened specimens and one of the ground specimens failed early on in the tests; the fatigue cracking initiated from defects still present at the weld toes after the dressing procedures had been carried out. A false "sense of security" arising from the use of these dressing techniques, therefore permitting higher operating stresses, may well lead to serious problems in commercial practice in the absence of appropriate controls and inspection.

Table 5.1 : (a) Specified compositional ranges of ROQ-tuf AD690 and BS 4360 grade 55E steels.

Steel	% Composition (maxima unless range stated).							
	C	Mn	Si	P	S	Nb	V	Mo
ROQ-tuf AD 690	.12-.21	.45-.70	.20-.35	.035	.04	-	-	.50-.65
BS 4360 55E	.22	1.6	.10-.60	.04	.04	.003-.10	.003-.20	-

Table 5.1 : (b) Specified mechanical properties of ROQ-tuf AD690 and BS 4360 grade 55E steels.

Steel	Specified properties (minima unless range stated).		
	Yield Stress (MPa)	Tensile Strength (MPa)	Charpy Impact Energy (J)
ROQ-tuf AD690	690	760-895	-
BS 4360 55E	450	550-700	61 (at -20^{o}C)

Table 5.2 : Summary of test data for stitch welded specimens.

Specimen	Steel type	Initiation stress range (MPa)	Cycles for initiation ($x10^6$)	Fatigue crack initiation sites
T1	55E	120	7.0	Weld roots
T6	AD 690	60	4.57	Weld toe and weld roots
T7	55E	60	2.68	Weld roots
T8	AD 690	60	1.59	Weld roots
T13	55E	70	2.27	Weld root
T14	55E	60	2.0	Weld root and weld toes

Note: In this Table and in Tables 5.3, 5.5, 5.6 and 5.7 to follow, the "cycles for initiation" refer only to the number of loading cycles imposed at the initiation stress range before cracking occurred.

Table 5.3 : Summary of test data for continuously welded specimens.

Specimen	Steel type	Initiation stress range (MPa)	Cycles for initiation ($x10^6$)	Fatigue crack initiation sites
T2	55E	80	1.89	Undercut defect
T3	55E	110	4.2	Weld toe
T4	AD 690	70	4.0	Undercut defect
T5	55E	130	4.8	Weld toe
T9	55E	140	1.0	Weld toe
T10	AD 690	80	1.0	Undercut defect
T11	55E	110	6.0	Weld toe
T12	AD 690	60	[illegible].0	Undercut defect

Table 5.4 : Summary of test results and specimen details in the initial investigation into the effects of microstructure

Specimen	Welding procedures and fatigue test results.
AD1	Welded after cooling to -25°C, so as to contain a hard heat affected zone. No cracking after 34 million cycles.
AD2	Welded so as to contain hard HAZ and undercut. Fatigue crack initiated after 8.8 million cycles at 50 MPa. After 25 million cycles, crack was 4 mm deep, 15 mm long.
AD3	Welded so as to contain undercut. No fatigue cracking after 34 million cycles, but two hot cracks present in final brittle fracture surface.
AD4	Welded so as to contain undercut. Very small fatigue cracks (less than 2 mm deep) in final fracture surface after 34 million cycles.
AD5	Welded so as to contain hard heat affected zone and undercut. Fatigue crack initiated at a stress range of 50 MPa. After 4.5 million cycles at 50 MPa and a further 3 million cycles at 40 MPa, fatigue crack 8 mm deep and 55 mm long.

Table 5.5 : Summary of test data obtained in the investigation of the mean stress effect

Specimen	Peak hardness (Hv)	Initiation stress range (MPa)	Cycles for initiation ($x10^6$)
DM1	370	60	8,18
DM2	430	50	4,90
DM3	420/440	70	2,83
DM4	380	60	3,84

Note: (1) The peak hardness in the near-heat affected zone should exceed 400Hv in order to simulate the service failure.

(2) Fatigue cracking occurred on both sides of the balance pad in specimen DM3, thus two peak hardnesses are recorded.

Table 5.6 : Summary of test data for ground specimens

Specimen	Steel/weld type	Initiation stress range (MPa)	Cycles for initiation ($x10^6$)	Fatigue crack initiation sites
T15	55E/E7018	210	2.0	Weld root
T16	55E/E7018	180	5.0	Weld root
T17	AD 690/E7018	170	1.5	Weld root
T18	AD 690/E7018	170	5.5	Weld root
T27	AD 690/309 L	150	2.47	Weld toe
T28	55E/309 L	170	6.5	Weld root

Table 5.7 : Summary of test data for peened specimens.

Specimen	Steel/weld type	Initiation stress range (MPa)	Cycles for initiation ($x10^6$)	Fatigue crack initiation sites
T19	AD 690/E7018	250	2.2	Weld root
T20	55E/E7018	280	3.0	Weld root
T21	AD 690/E7018	230	5.0	Weld root
T22	55E/E7018	220	3.0	Flame cut edge
T23	55E/E7018	200	2.5	Weld toe
T24	55E/309 L	240	7.4	Weld root
T25	AD 690/309 L	240	5.74	Weld root
T26	55E/309 L	240	3.64	Weld root
T29	AD 690/309 L	230	3.0	Weld toe

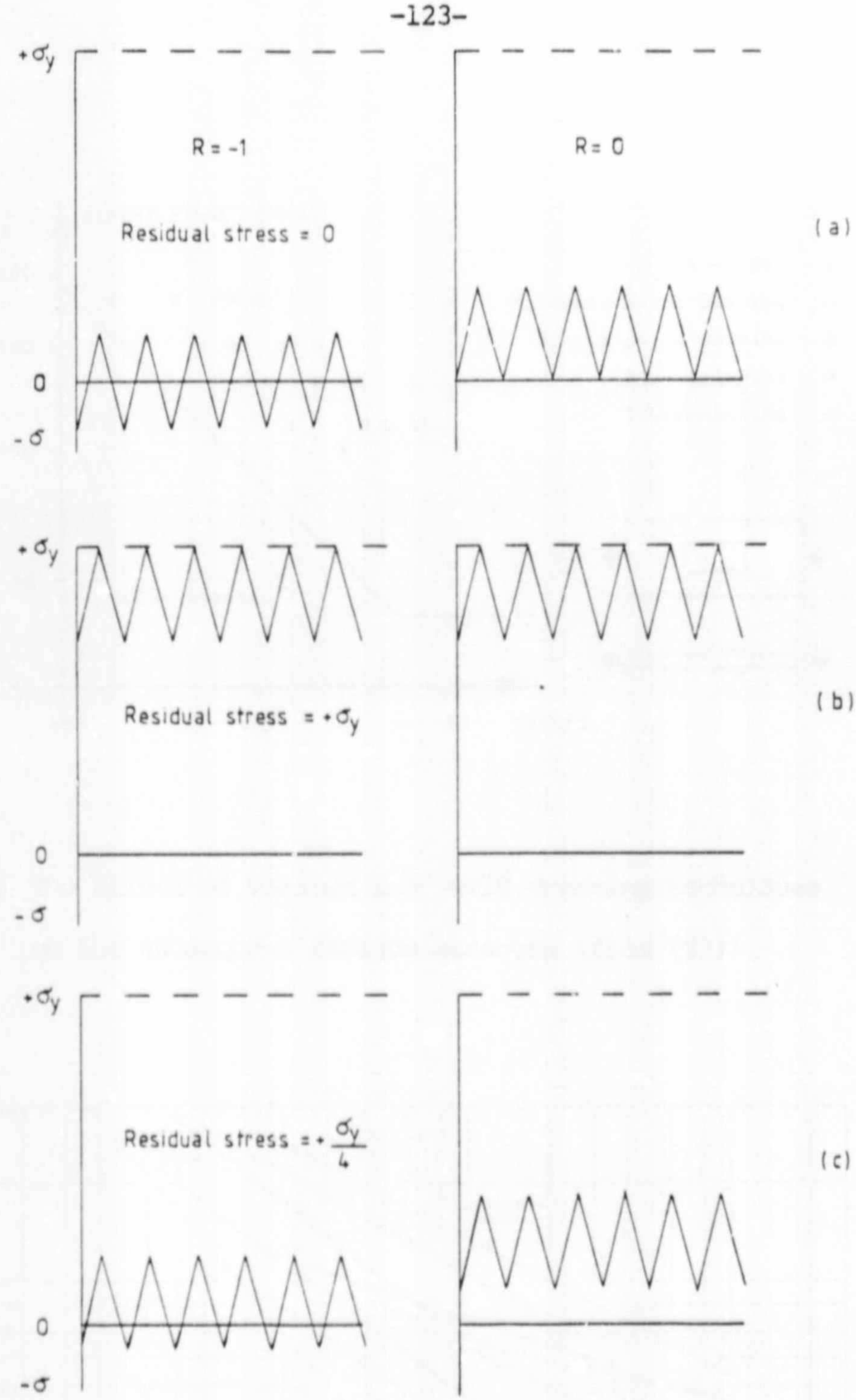

<u>Figure 5.1</u> A schematic illustration of (a) fully reversed and fully tensile loading (b) the effect of a tensile residual stress and (c) the two loading conditions after a thermal stress relief.

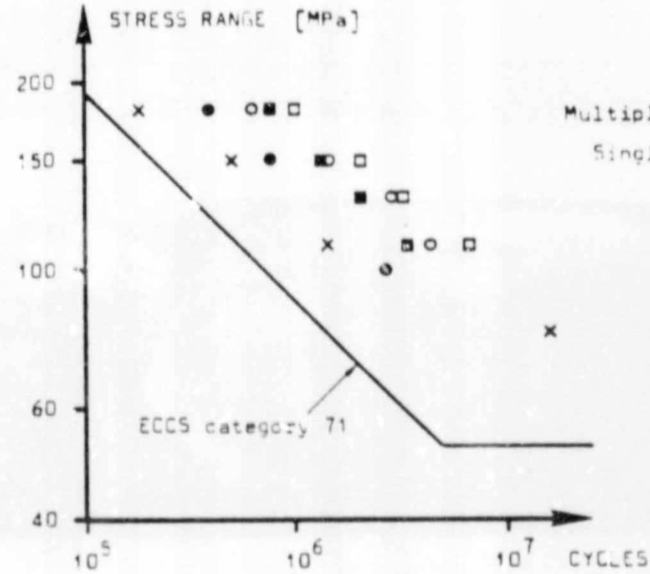

<u>Figure 5.2</u> The effect of various post weld [illegible]ssing techniques on the subsequent fatigue strength (from (22)).

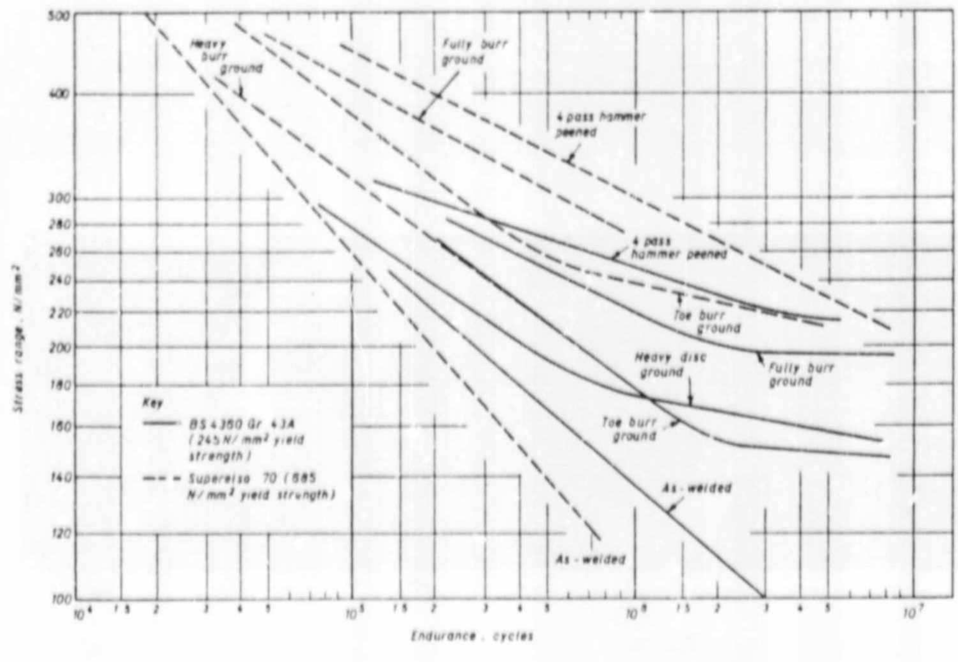

<u>Figure 5.3</u> A comparison of the effects of grinding and peening on the fatigue strength of fillet welded joints (from (20)).

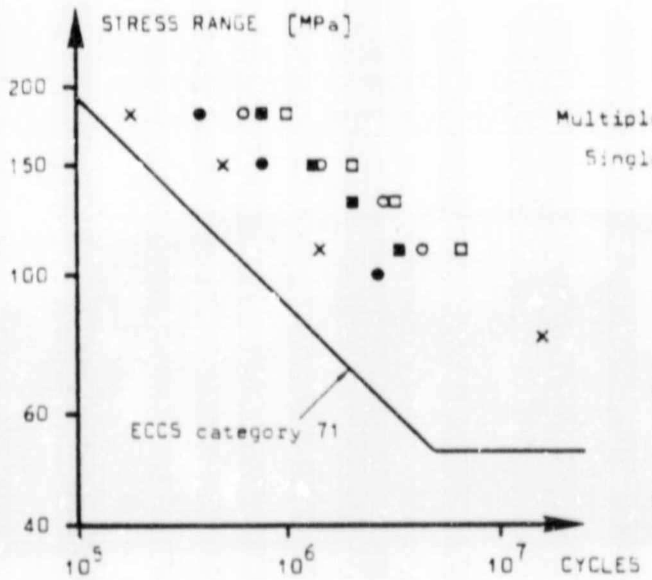

Figure 5.2 The effect of various post-weld dressing techniques on the subsequent fatigue strength (from (22)).

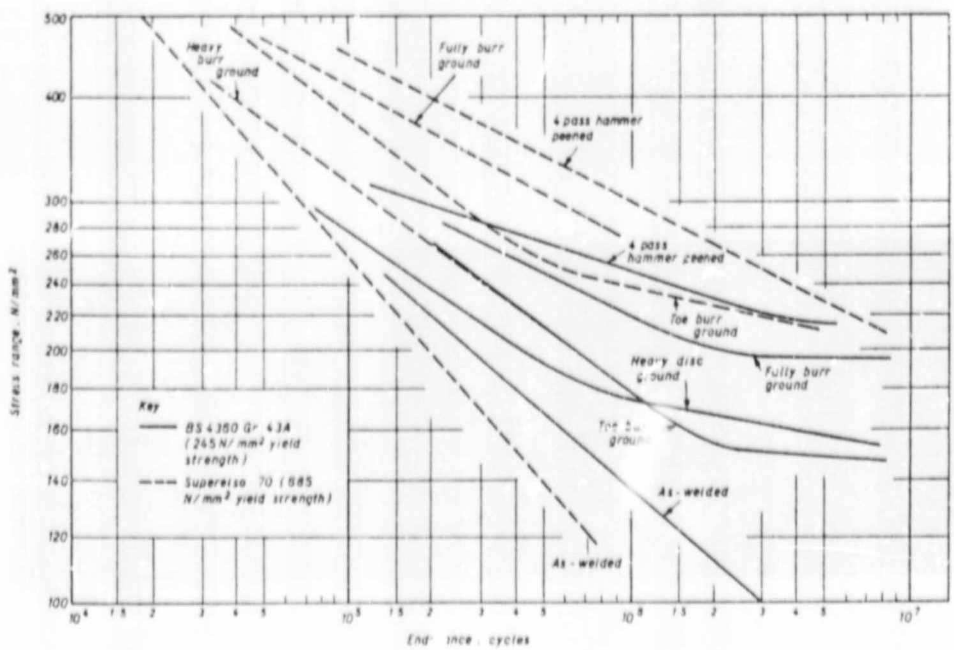

Figure 5.3 A comparison of the effects of grinding and peening on the fatigue strength of fillet welded joints (from (20)).

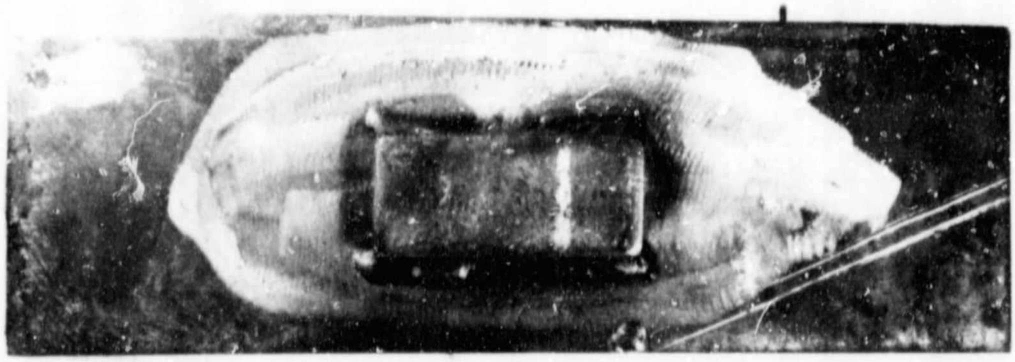

Figure 5.4(a) Specimen simulating the old stitch welded balance pad.

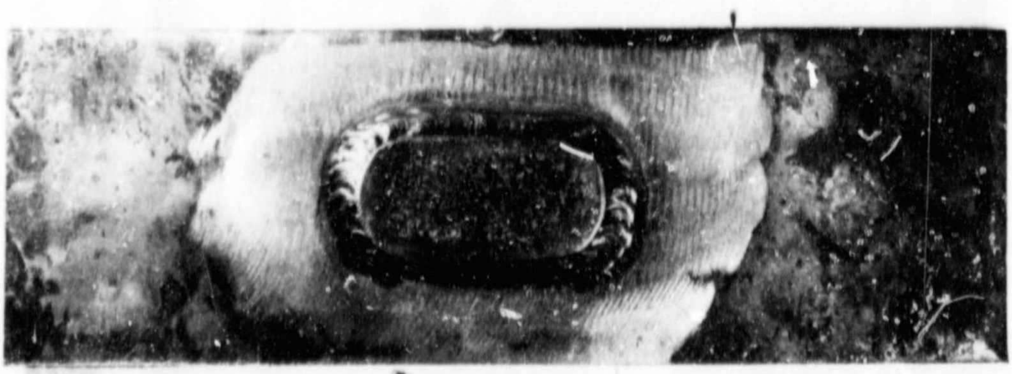

Figure 5.4(b) Specimen simulating the new continuous balance pad weld.

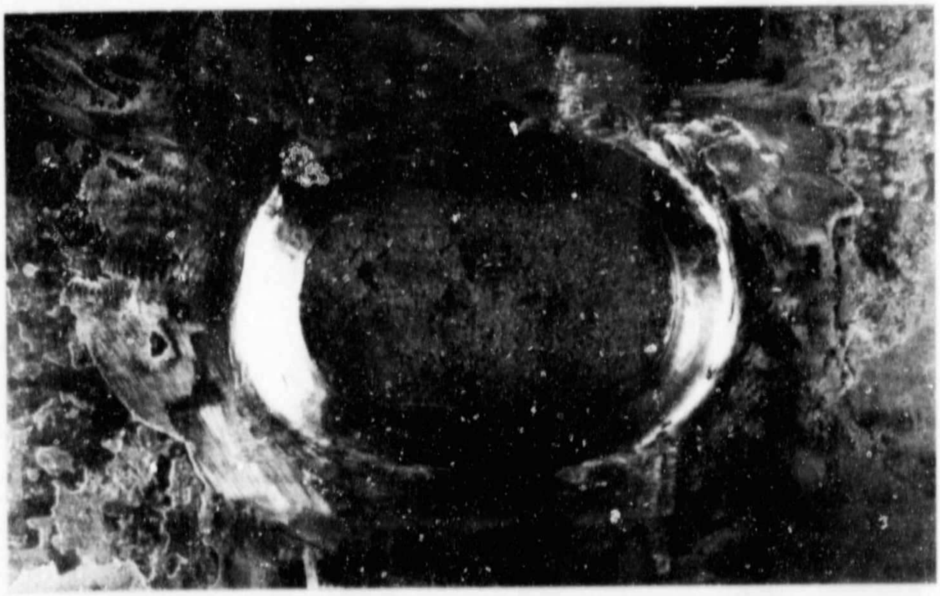

Figure 5.5(a) Continuous-type balance pad specimen, with the weld fully ground

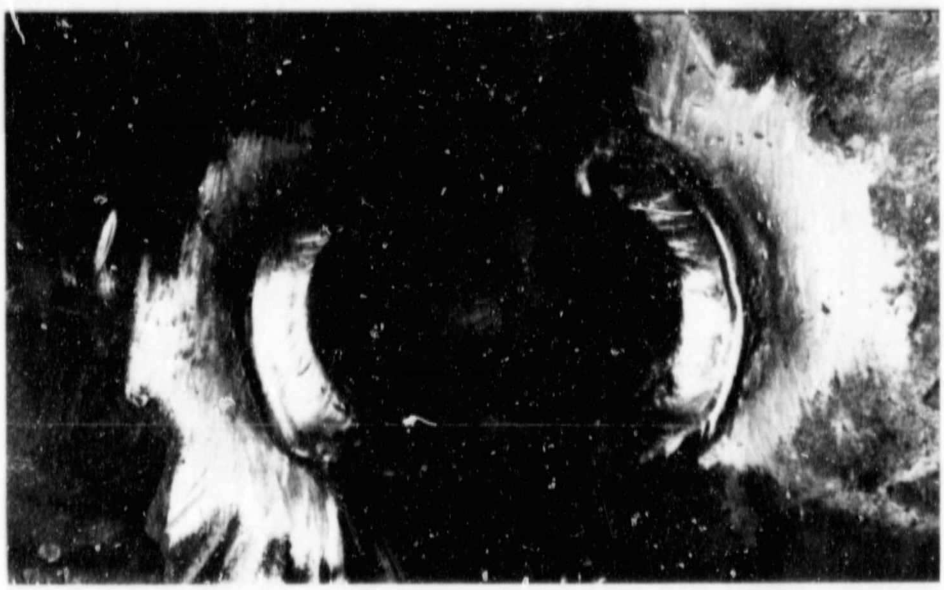

Figure 5.5(b) Continuous type balance pad specimen with the weld toe hammer peeened.

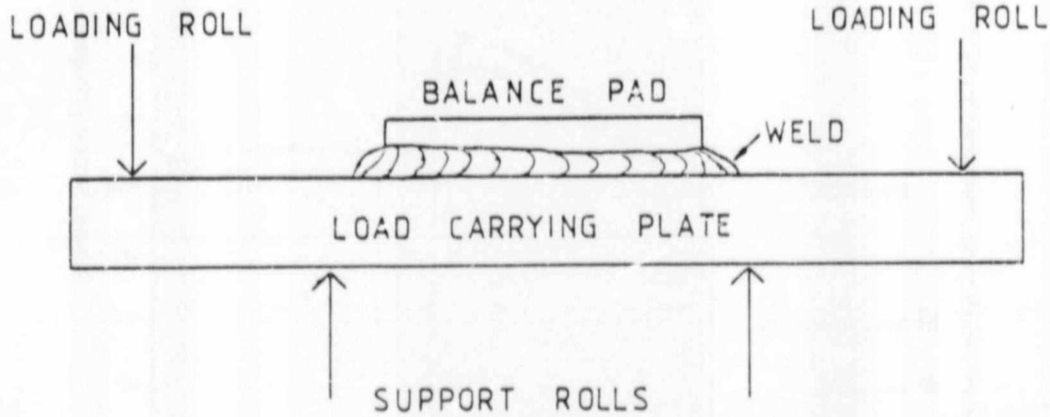

Figure 5.6 A schematic diagram of the four point bend test fixture. Note that the balance pad weld is on the tensile surface.

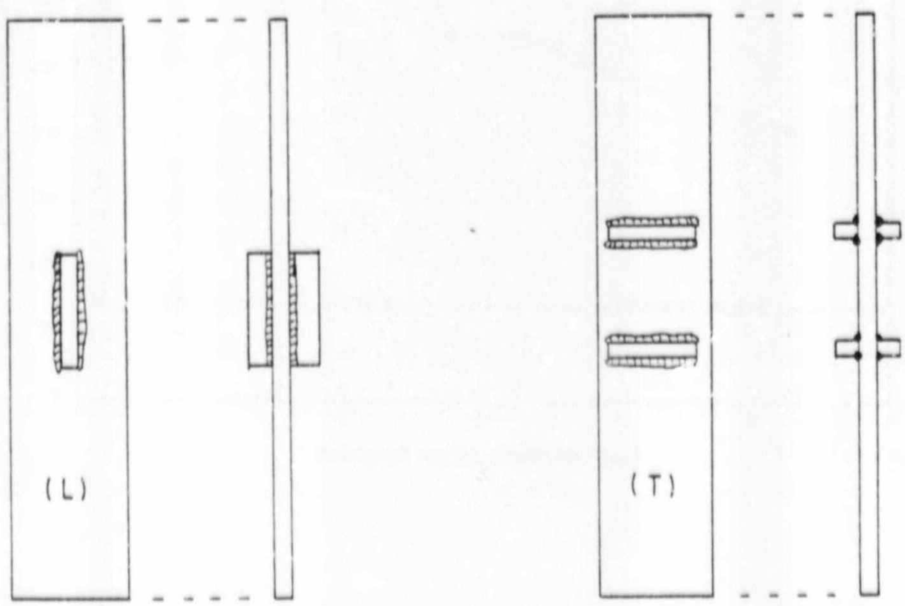

Figure 5.7 The longitudinal (L) and transverse (T) welded stiffeners investigated by Gurney (12). Note the similarity to the stitch and continuous type balance pad welds respectively.

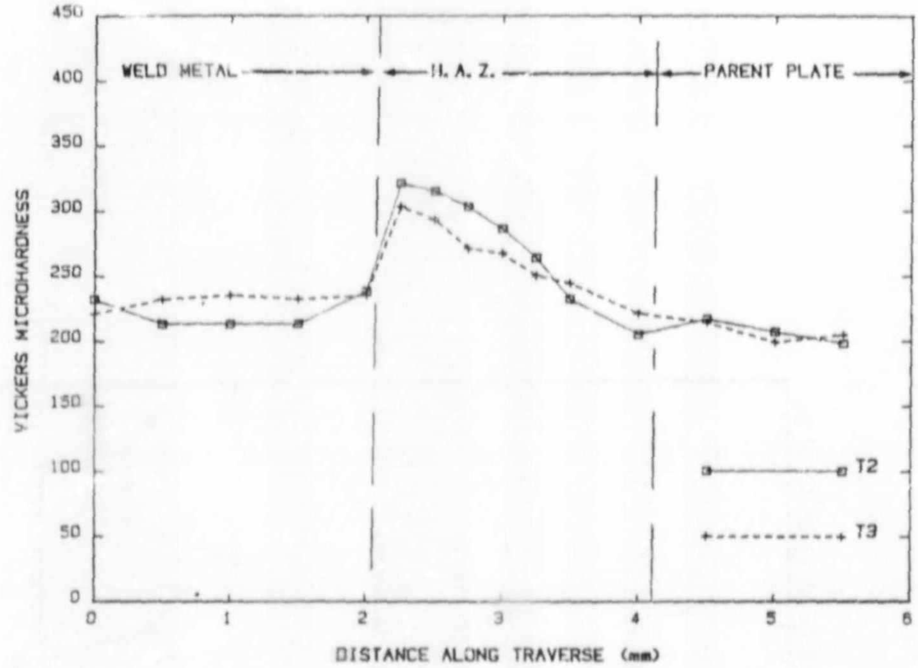

(a)

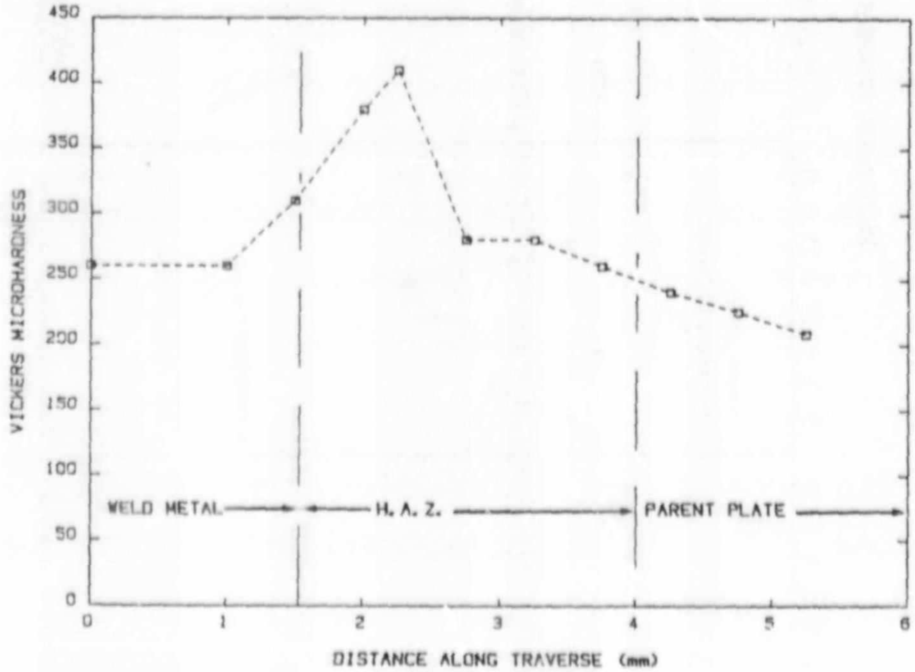

(b)

<u>Figure 5.8</u> A graphical summary of the results obtained in the microhardness traverses across (a) specimen balance pad weldments and (b) the service failure (104).

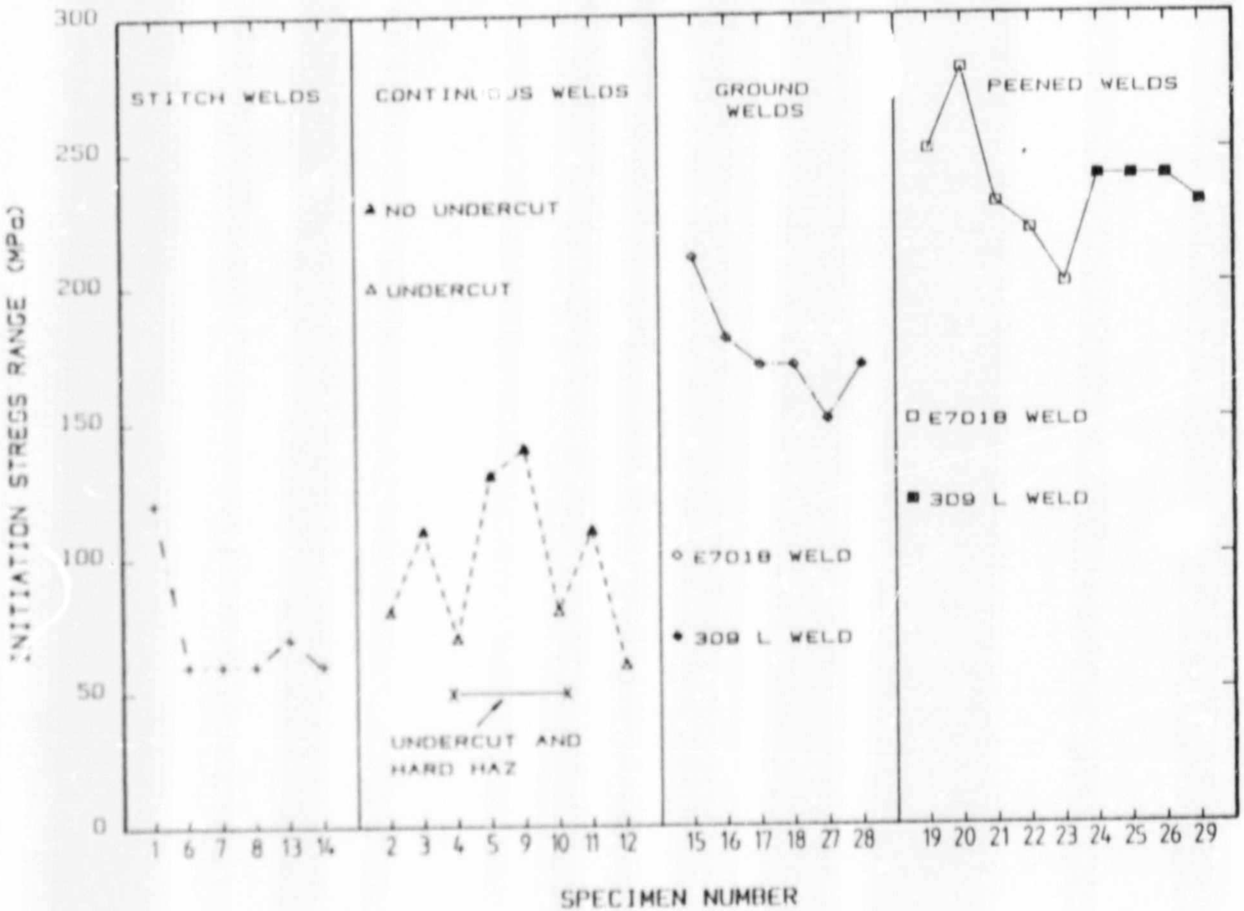

Figure 5.9 A graphical summary of the results obtained in the fatigue tests, clearly illustrating the beneficial effects of grinding and peening.

CHAPTER SIX

CRACK INITIATION SITES, CRACK SHAPE DEVELOPMENT AND CRACK GROWTH RATES OBSERVED IN THE FATIGUE TESTING OF FILLET WELDED JOINTS

6.1 Introduction and Background

6.1.1 Typical fatigue crack initiation sites in welded joints

The previous Chapter detailed the results obtained in the endurance limit testing of specific fillet welded details, and it was shown in this work, consistent with related published work, how small defects at the toes of what would normally be considered "good welds" caused a drastic reduction in the fatigue strength of that weld (12,95,99,104,106-111). It should be noted however, that all weld joint configurations cause stress concentrations, and are therefore likely to provide preferential crack initiation sites (18). In this reference document, welded details are essentially one of two types, and either perpendicular (transverse) or parallel (longitudinal) to the direction of loading.

In as-welded longitudinal details, the fatigue cracking is likely to initiate from stop-start positions, weld ends, or if these are not present, at weld surface ripples (18). If these preferential initiation sites are removed, by grinding the weld flush for instance, fatigue cracking would be associated with weld defects (18). In transverse butt welds, fatigue cracking is associated either with the welds ends or the weld toe. The fatigue strength of this detail is determined by the weld shape and can therefore be improved by grinding the whole weld flush with the plate surface. In such a case fatigue crack initiation would occur either from the weld root or from weld subsurface defects (18). In transverse fillet welds, fatigue cracking either occurs at the weld toe and propagates into the stressed member, or at the weld root and propagates into the weld (18).

Thus it is clear that in all cases, the local conditions of the weld ends or weld toes are the prime factor in determining the fatigue strength of any welded joint. Signes et al.'s initial work in this field (13) indicated that the crack-initiating defects in welds made from a rutile coated manual metal arc electrode were either undercut or slag intrusions located at the edge of the weld metal. It was therefore considered that the welding process itself may be the prime cause of the defects, and to eliminate the incidence of defective welds, other welding processes should be considered (99). Related studies (112-114) therefore evaluated various MMA, TIG, MIG and SA welding techniques and consumables, but it was shown that all processes produced some weld toe defects, although the weld pool turbulence was an important contributory factor in the number and type of these defects. This work (112-114) therefore served to confirm, as shown in the preceding Chapter, that post-weld dressing techniques are the most effective method of removing weld toe defects, and therefore in improving the fatigue strength.

This therefore indicates that, in order to fully understand the variations that may occur in fatigue testing of weldments, it is necessary to identify the crack initiation point in each specimen, and relate this to the result of test.

6.1.2 Crack shape development and crack monitoring

The fatigue crack shape developed in any specimen is a function of the specimen geometry and the loading arrangement; thus fatigue cracks will have a "preferred propagation path", and tend to an equilibrium shape (115-119). The crack shape developed in any specimen is different when the applied loading is pure tensile as compared to that in the same specimen under bending loads, as shown in Figure 6.1 (115,116). In the case of pure tensile loading of finite thickness plates, the cracks grow in a near semi-circular shape until the depth is greater than the half-plate thickness, whereupon the cracks elongate to a semi-elliptical shape (115). In bending fatigue, the crack shape development is less well understood, although it is clear that there is a preferential propagation path (115). An obvious complicating factor in bending is the stress distribution, which will change from tensile to compressive across the plate thickness, as described earlier in Chapter Three. Clearly, there can be no tensile stress across a crack, and thus the peak tensile stress will exist along the crack front. Obviously, if the crack is not full width, the exact value of the applied stress along the crack front will vary, from a maximum at the deepest part of the crack, to a minimum at the surface.

However, fatigue crack growth is further complicated by the fact that the initial crack shapes are strongly dependent on the initiating notch geometry, and thus the preferential propagation path can only be defined when the crack has grown away from the influence of the starter notch (116,118,119). This is illustrated in Figure 6.2 which shows the change in crack shape in bending fatigue as a function of the configuration of the starter notch (119). In this work, two general types of starter notches; those with a large depth to width ratio (denoted by numbers 3, 8, 10 and 17 in Figure 6.2), and those with a shallow depth to length ratio (7 and 12 in Figure 6.2) were used to investigate the subsequent changes in shape of the fatigue crack. It will be noted that there is a wide variation in early crack shapes, but this range decreases as the crack depth increases, such that the different growth patterns converge to a single line. It must therefore be expected that, in the fatigue testing of weldments, there will be some considerable scatter in the early crack shapes, due to the different initiating defect shapes.

Fatigue crack growth rates in weldments must, of necessity, be measured either by indirect means such as the potential drop methods, or by marking the crack front at various stages during the propagation, by heat-tinting or beach-marking. This is because, at most, only the crack surface length is visible at all stages during propagation. Thus, it would only be possible to evaluate the crack depth if the exact relationship between the two parameters were known at all stages in the propagation. From the foregoing, however, it is clear that this is not well established, due to the dependence of the early growth shapes on the initiating defect. In addition, in the case of crack initiation from the weld root, even the crack surface length will not be visible.

Potential drop techniques entail passing a constant current through a test specimen and measuring the disturbance of the potential field caused by the crack. As the crack depth increases, the potential measured across the crack increases. Potential drop methods for monitoring crack extension in fracture and fatigue specimens have been extensively investigated, as will be discussed in Chapter Seven, to follow. Measurements of the depth of surface cracks in plain plate specimens using the potential drop method have also been developed (see for example, references 120-122). These particular methods appear to reproducibly and reliably predict crack depth to within ± 18% (120), ± 0,15mm (121) and ± 0,04mm (122).

However, when dealing with weldments, there are two problems associated with crack depth monitoring using the potential drop method, and both relate to the nature of the specimen. In the first instance, the exact location of the crack initiation site is not known, and if the potential drop probes do not straddle this initiation site, the initial stages of crack propagation will not be detected. Indeed, this is one of the main reasons for the controversy that exists as to the exact proportion of fatigue life of a welded joint that is spent in initiation (123). The other problem arises due to the surface profile of a welded specimen. Even if the probe spacing can be reproduced on different specimens by using a template, the electrical spacing (the actual surface distance between contacts) may be different, as illustrated schematically in Figure 6.3 (123). This can be overcome to some extent by normalising the initial voltage readings with an average initial reading for a given set of specimens, but can still be a major source of error, especially in the initial stages of growth (123).

In addition, it is clear that the crack front will have to be marked at various stages during the propagation in order to calibrate the potential drop method used. This can be done by controlled load changes, such that the changes of crack growth rate can be observed as a series of light and dark bands, or beachmarks, which define the position of the crack front at each of the programmed load changes (119,124,125). In order to produce a distinct beachmark, however, it is necessary to decrease or increase the stress range, maintaining a constant maximum stress throughout, and some considerable experimentation may be necessary before the fracture surface shows the required markings (121). These significant changes in crack growth rates may have some effect on the results of the test as a whole.

The crack front can also be marked at various stages during the propagation by heat-tinting the specimen, which results in differential oxidation, and a series of temper-colours across the fracture surface indicate the relative crack front positions during the test (117). This method can only be used a limited number of times for a given specimen, otherwise it is difficult to distinguish between the different temper colours, particularly during the early stages of growth. Compared to beachmarking, however, it has been shown that heat-tinting does not affect the crack propagation rate (117).

6.1.3 Calculation of crack tip stress intensities

Various solutions are available for the description of the stress intensity factor (K_p) for a surface crack in a plain plate specimen (defined here as K_p). These solutions (see, for example, references 115,118,126) have the general form:-

$$K_p = F(a/c)\, F(a/t)\, F(a/w)\, \sigma \sqrt{\pi a} \qquad (6.1)$$

where a is the crack depth, c the crack half-length, t is the plate thickness and w is the plate width. Thus, the accuracy with which the stress intensity at the crack tip can be calculated is dependent on accurate measurements of crack depth and length, which define the various correction factors F(a/c), F(a/t) and F(a/w).

However, these solutions obviously cannot be applied to welded specimens, because of the additional stress concentrating effect of the weld, which will have a significant effect on the early growth of the crack. Clearly, in order to fully assess the fatigue life of weldments, it is important to evaluate the stress concentration and the stress distribution at the weld toe. Thus finite element analyses have been performed (127-130) on specimen weldments in order to establish the magnification factor, M_k such that the stress intensity of a surface crack, initiating from a weld (K_w) may be evaluated:

$$K_w = M_k K_p \tag{6.2}$$

The stress intensity solution proposed by the (UK) Welding Institute (128-130) was used in this test programme, and has the general form:-

$$K_w = M_k \frac{M_s M_t M_p}{\phi_o} \sigma \sqrt{\pi a} \tag{6.3}$$

In equation (6.3), M_k is the correction for the stress concentrating effect of the weld toe, M_s is a correction factor to allow for the effect of a free surface at the crack mouth, M_t is a correction factor to allow for the presence of a free surface ahead of the crack (or a finite thickness correction), and M_p is a correction factor to allow for the crack tip plasticity, and is dependent on the plastic zone size. (These factors have been given the symbol M to signify that they are magnification factors). However, M_p will be small for fatigue crack propagation under nominally elastic stresses, and therefore can be ignored in most fatigue situations (128).

ϕ_o is the complete elliptical integral of the first kind, more often designated E_k, and specific values of this parameter can be obtained from standard tables (..1), provided that the crack depth (a) and the crack length (c) are known. However, the Welding Institute method is to treat M_s, M_t and ϕ_o as a single overall magnification factor, and values of this may be obtained directly from a graphical solution (128), reproduced here as Figure 6.4. It can be seen that in order to evaluate this magnification factor, it is necessary to have accurate values for crack depth and length.

The original analysis (128) of M_k was subsequently revised in order that it would cater for a wider range of weld sizes and plate thicknesses (129,130); however, all these analyses predicted that the magnitude of M_k decreases rapidly with increasing crack depth. This is consistent with its definition, since this factor is the difference in stress intensity for a surface crack in a plain specimen and that in a welded specimen, as indicated in equation (6.2). Thus, as the distance of the crack tip from the weld increases, the stress concentrating effect of the weld is reduced.

6.1.4 Summary

This Section has described the typical crack initiation sites that would be observed in fatigue failures of welded joints. In general, fatigue crack initiation is associated with weld ends, weld toes, or stop-start positions; if these are ground flush with the surface of the stressed member, typical initiation sites are weld roots, or weld defects. Thus, the fatigue performance of any welded joint must be evaluated in conjunction with an examination of the fracture surface, in order that the initiation point can be located, and correlated with the fatigue strength of that joint.

The equilibrium crack shapes have been outlined, and it has been shown that, although the crack shape is consistent for a given set of specimens, under a given set of loading conditions, the early crack shapes are strongly dependent on the initiating defect. Thus, in order to monitor crack growth, it is necessary to use indirect methods, such as potential drop, since evaluation of crack depth from a measurement of the surface length can give significant errors. However, the accuracy of potential drop techniques are also affected by the presence of a weld, and it is necessary to calibrate the method either by marking the crack front at various stages during propagation, or by terminating tests at different times after initiation, so that the crack growth pattern may be established.

It was further shown that, in order to calculate the stress intensity at the crack tip, accurate measurements of both crack depth and crack length are required. It should be noted here that the stress intensity calculation outlined in Section 6.1.3 is only applicable to situations where the crack initiates at the weld toe.

The following Sections in this Chapter detail the initiation sites, crack shape development and crack growth rates observed in the endurance limit testing of various fillet welded details.

6.2 Experimental Details

As detailed in the previous Chapter, all specimens were tested under four point bending conditions, since this simulated the operating conditions more accurately than direct tension loading. (A schematic of the loading arrangement is shown in Figure 5.6). A 100 kN Amsler Vibrophore fitted with a Howden load controller was used for all tests, and starting frequencies of between 120 and 140 Hertz were achieved.

In all tests, the Amsler Vibrophore was set to run for 10 million loading cycles (or approximately 22 hours of continuous testing) at a predetermined stress range, after the initial start-stop load cycles had been imposed. In the event of any fatigue crack initiation, the specimen compliance increases, thereby decreasing the test frequency and the machine is stopped automatically. The frequency cut-off could be set such that the machine would trip after only a small amount of crack propagation had occurred, and thus the number of cycles required for initiation could be recorded. In addition, as the crack grew through the specimen, the frequency would decrease, and this was also recorded, in an attempt to monitor crack growth with increasing compliance. If crack initiation did not occur within this first 10 million loading cycles the stress range was increased by 10 MPa; this incremental increase in stress range was repeated every 10 million cycles until crack initiation was observed. Thus, the endurance limit of each detail was defined in this work as the highest stress range at which crack initiation did not occur within 10 million cycles.

In addition to using the frequency monitoring module in the Howden load controller, crack initiation (and subsequent propagation) was monitored using a direct current potential drop (DCPD) system comprising a Gould constant current supply and a high resolution Fluke digital voltmeter. The potential drop was measured by spot welding pairs of Nichrome wires on either side of the expected crack initiation sites; the current leads were mechanically attached to the specimen remote from the weld (see Figure 6.5).

In order to correlate the potential drop and frequency changes with crack advancement, the crack front was marked at intervals during the propagation. Initially this was carried out by heat-tinting (10 minutes at 500^{o}C), which resulted in various temper-colours on the fracture surface (107). However, it was found that a particular specimen could only be heat-tinted at most four times, otherwise it was found difficult to distinguish the early crack shapes. Specimens were therefore subjected to load changes during the propagation stage, providing characteristic beach marks on the fracture surface (108,110). In order to produce a clear beach mark, it is necessary to increase or decrease the stress range significantly, but maintain a constant maximum stress. Such a change in the loading conditions inevitably gave rise to a change in the operating frequency of the system; this complicated the correlation between frequency change and crack depth somewhat. Obviously, if beach marks are to be produced by reducing the stress range, it is necessary to monitor the potential drop across the crack surface to ensure that crack extension has in fact occurred.

In the case of the dressed welds, it was seen that the crack initiation site was removed from the weld toe to the weld root, ie. the crack initiation became subsurface. Furthermore, the crack propagation occurred on different fronts, only establishing the semi-elliptical equilibrium crack shape across these separate fronts after some considerable crack extension had occurred. Accordingly, the tests on the ground and peened welds were terminated at different stages (for example, one after 10 million cycles after initiation had occurred, one after 2 million cycles after initiation, and one immediately after initiation). Thus the fatigue crack front could be seen at the different stages, and the typical crack propagation path was established.

6.3 Results and Discussion

6.3.1 Preferential crack initiation sites.

Crack growth generally occurred on both sides of the stitch welded attachment, and initiation typically occurred at the root of the weld, at the corner of the balance pad, as shown in Figure 6.6 (a). However, there were some instances of crack initiation from the weld end due to undercutting, as shown in Figure 6.6 (b). In the cases of weld root initiation, the preferred crack path through the weld metal was inclined at an angle towards the centre of the attachment, but as the cracks grew into the main load carrying plate, the growth became normal to the plate surface. This growth pattern has been noted elsewhere (96).

In the undressed, continuously welded specimens, initiation occurred at the weld toe in all cases, and cracking only occurred on one side of the attachment. It was seen that a high initiation stress range (100 MPa or greater) was required in the absence of any undercut at the weld toe. The fracture surfaces of these specimens showed multiple initiation points at the weld toe, as indicated in Figure 6.7 (a). Such "ratchet markings" are indicative of a relatively low stress concentration. The fracture surfaces of the specimens that recorded low endurance limits (less than 80 MPa) indicated that initiation had occurred at an undercut defect at the weld toe, as shown in Figure 6.7 (b).

In the ground and peened specimens, initiation typically occurred at the weld root, as shown in Figure 6.8 (a) However, if the weld had been insufficiently dressed, initiation could still occur from weld toe defects, as shown in Figure 6.8 (b). In some instances, fatigue crack initiation occurred at the edge of the main load-carrying plate remote from the weld. (The specimens had been flame cut, and the sides were not machined before testing). As previously mentioned, it has been shown (95) that micro-cracking can result from even high quality gas cutting; the effectiveness of the mechanical dressing procedures was most clearly illustrated by such cases of initiation remote from the weld.

6.3.2 Crack shape development.

The results detailed in this Section refer only to the continuous welds that were not dressed by grinding or peening. This is due to the fact that the dressed welds showed multiple crack propagation paths, and subsurface initiation, as already mentioned in Section 6.1.3. This latter point complicated the potential drop work, since, as the probe pairs have to straddle the crack, the spacing had to be much greater for these welds; consequently, the potential drop monitoring system was less accurate. In addition, the weld root initiation would greatly complicate the calculation of the cyclic stress intensity, even if the change in crack depths and lengths across these multiple crack fronts could have been evaluated. Thus, these dressed specimens were not subjected to any programmed load changes in order to mark successive positions of the crack fronts.

Instead, the typical crack path in the ground and peened specimens was traced by stopping selected tests at different stages after crack initiation, and Figure 6.9 is a schematic representation of the crack propagation pattern. Firstly, the crack initiates at the root and propagates upward to the surface of the weld. Thereafter, the crack propagates on two separate fronts, downwards from the welds on the side of the balance pad, into the load bearing plate.

Figure 6.10 shows the data obtained in this test programme for the change in crack depth (a) with surface length (2c). A straight line was best-fitted to this data with a regression coefficient of 0.99. However, as indicated in this Figure estimating the crack length for a crack depth of 7.5 mm (for example) could give an error of approximately 20 mm. Additionally, there is little data for small crack depths, and the best fit straight line does not pass through the origin. Figure 6.11 shows the change in crack aspect ratio (a/2c), in relation to the change in fractional crack depth (a/t). This graph does not show the same linear dependence as Figure 6.10, but as noted in Section 6.1.2 the crack shape during the initial stages of propagation (low a/2c or low a/t, or both) is strongly dependent on the initiating flaw. However, for a/t greater than about 0.5, the scatter is much reduced, as indicated by the lines enveloping the data in Figure 6.11. This is consistent with the results shown in Figure 6.2 which were obtained in the fatigue testing of samples which were machined in such a way as to contain a wide variety of initial notch shapes (119). Thus, it is to be expected that, since the results shown in Figure 6.10 and 6.11 were obtained from a total of ten welded samples, and the the growth patterns will be different, due to the differing initiating notch shapes.

6.3.3 Crack Growth Rates.

The potential drop was monitored throughout each test, and gave an indication of crack initiation, as well as the position and the relative extent of the crack.

The change in voltage, as measured for the continuously welded, undressed specimens, is plotted against the crack depth in Figure 6.12. It will be noted that there is some scatter in these results, since, as detailed in Section 6.1.2, it is virtually impossible, even with a template, to have reproducible electrical spacings (96). In addition, if one pair of potential drop probes did not straddle the initiation point, the potential drop did not change immediately upon initiation. However, the data presented in Figure 6.12 does indicate that, for cracks deeper than about 3 mm, the change in the potential can be used to monitor crack extension, although exact measurements of crack growth rate are not possible.

Initially it was envisaged that the change in operating frequency of the resonant fatigue test facility could be used to monitor crack growth. However, the method of marking successive crack fronts affected these results, since a change in operating stresses immediately affected the operating frequency (before any further crack advance occurred). However, the results that were obtained for the heat-tinted specimens are shown in Figure 6.13 (a) where the change in frequency is plotted against the normalised crack surface area, and in Figure 6.13 (b) the frequency change is plotted against the crack depth, for the same specimens. This was done since the frequency change is affected by the increase in specimen compliance, and it was considered that this would be a function of the total uncracked area rather than the remaining ligament (or crack depth). Thus, the results shown in Figure 6.13 (a) were obtained by calculating the crack surface area, for each stage in the crack propagation, by assuming the crack shape to be a semi-ellipse.

However, there is some considerable scatter in both these graphs, and this is ascribed to errors in crack depth and length measurements and the different initial crack shapes. In addition, the fact that the specimens had to be removed from the test machine in order to be heat-tinted could have caused some variation in the operating frequency of this resonant test facility. It is therefore clear that, in order to establish the exact correlation between frequency change and increasing crack depth or crack surface area, it will be necessary to devise some way of marking the crack front that does not entail changing the applied load conditions, or removing the specimen from the machine. Such a correlation could possibly be achieved with a set of specimens that are identical, with identical preferred crack propagation paths, and stopping each test at a different stage after initation. The different crack surface area (or crack depth) in each specimen could then be easily correlated with the change in frequency. Unfortunately, it is doubtful that such a correlation would be of any use in the fatigue testing of weldments!

Crack tip stress intensities were evaluated as outlined in Section 6.1.3, and the corresponding rate of change in crack depth were calculated for the specimens in which the crack fronts were beach marked, and the results are shown in Figure 6.14. There does appear to be some scatter in these results, but it must be indicated that, at these low crack growth rates (less than 10^{-8} m/cycle), any error in measuring the crack depths will be magnified on such a plot. Additionally, the method used to mark the successive crack fronts would give rise to some scatter in the crack growth rates, since to produce a distinct beach mark, it was found necessary to either double or halve the previous stress range. Thus, there could be some crack retardation when changing from a high stress range to a low stress range.

Additionally, it will be noted that the results obtained in this test programme lie outside of the scatterband for cruciform joint specimens, tested in air to validate the proposed stress intensity solution (128). This is due to the fact that the tests reported here were carried out under four-point bending, whereas the Welding Institute performed their tests (128) under direct tension. It will be recalled from Section 6.1.3 that the stress intensity is evaluated from both the crack depth, a, and the surface length, 2c. It will further be recalled from Section 6.1.1 that the fatigue crack shape adopted under bending is different to that due to tensile loading. Indeed, as shown in Figure 6.1 (a), under tensile loads the crack aspect ratio (a/c) tends to 1,0 as the fractional